



Contents lists available at SciVerse ScienceDirect

## Earth and Planetary Science Letters

journal homepage: [www.elsevier.com/locate/epsl](http://www.elsevier.com/locate/epsl)

## Thermal evolution of Earth with xenon degassing: A self-consistent approach

Catherine M. Padhi<sup>a</sup>, Jun Korenaga<sup>b,\*</sup>, Minoru Ozima<sup>c</sup><sup>a</sup> Calhoun College, Yale University, New Haven, CT 06520, USA<sup>b</sup> Department of Geology and Geophysics, Yale University, New Haven, CT 06520, USA<sup>c</sup> Department of Earth and Planetary Science, University of Tokyo, Tokyo, Japan

## ARTICLE INFO

## Article history:

Received 7 March 2012

Received in revised form

5 June 2012

Accepted 7 June 2012

Editor: T.M. Harrison

## Keywords:

Mantle convection

Heat-flow scaling

Thermal budget

Urey ratio

## ABSTRACT

We present a coupled atmosphere–mantle evolution model to investigate a possible connection between the present-day atmospheric budget of radiogenic xenon and the evolution of subsolidus mantle convection since the Hadean. Two different types of heat-flow scaling for mantle convection are tested; whereas a conventional scaling predicts more vigorous convection in the hotter past, a recent one predicts more sluggish dynamics. Extensive degassing expected for a putative magma ocean in the very early Earth as well as considerable atmospheric loss caused by an early intensive solar wind are taken into account by using an effective closure time. The success of modeling results is measured by how closely they can reproduce the present-day abundances of  $^{129}\text{Xe}^*$  and  $^{136}\text{Xe}^*$  in the atmosphere. The conventional scaling demands the present-day mantle to be highly radioactive, which in turn indicates a high initial abundance of  $^{244}\text{Pu}$ , and because the mantle is very efficiently processed with this scaling, a large amount of plutogenic  $^{136}\text{Xe}^*$  is predicted to have been degassed into the atmosphere. Various parameter uncertainties are explored by Monte Carlo sampling, and our modeling results suggest that the use of the conventional scaling leads to > 300% overprediction of the atmospheric  $^{136}\text{Xe}^*$  budget, whereas we can satisfy the xenon budget more easily with the recent scaling.

© 2012 Elsevier B.V. All rights reserved.

## 1. Introduction

Earth's atmosphere is mostly a product of volcanic degassing from the solid Earth (e.g., Pepin, 2006). The rate of volcanic degassing is controlled by the rate of mantle melting, which is in turn related to the vigor of mantle convection. The evolution of the atmosphere has thus a close connection to the thermal evolution of the mantle, and a number of previous studies have investigated this connection (e.g., Hamano and Ozima, 1978; Sleep, 1979; Allegre et al., 1987; Williams and Pan, 1992; Tajika and Matsui, 1993; Albarède, 1998; Porcelli and Turekian, 2003; Coltice et al., 2009).

A conventional view on the long-term evolution of mantle convection has been that the mantle was convecting more vigorously when it was hotter than present (e.g., Schubert et al., 1980; Davies, 1980; Schubert et al., 2001), though this view is also known to be incompatible with the present-day thermal budget of Earth (e.g., Christensen, 1985; Lyubetskaya and Korenaga, 2007b). During the last decade, a new scaling of mantle convection, which takes into account the effects of chemical differentiation on mantle rheology, has been developed and shown to be

able to explain the thermal evolution of Earth and its present-day thermal budget simultaneously (Korenaga, 2003, 2006). The new scaling suggests that mantle convection may have been more sluggish in the past because a greater degree of melting in a hotter mantle would make the mantle stiffer by more pervasive dehydration, and this notion of more sluggish convection in the past has been suggested to be consistent with available geological and petrological data (e.g., Bradley, 2008; Herzberg et al., 2010).

This new view on the evolution of mantle convection is radically different from the conventional one, so it is important to explore its implications for atmospheric evolution. The main purpose of this paper is therefore to compare the old and new scalings of mantle convection in terms of their predictions for the degassing history of Earth. We focus on xenon degassing for the following reasons. First, xenon is one of noble gases and thus chemically inert, so modeling its degassing is relatively straightforward. Being the heaviest noble gas, degassed xenon would forever stay in the atmosphere except during the very early phase of the solar system with an intense solar wind. In contrast, helium would escape into space with  $\sim 1$  Myr residence time in the atmosphere. Second, some xenon isotopes are radiogenic with their parent isotopes inside the solid Earth, helping us to constrain the temporal evolution of the coupled atmosphere–mantle system. Finally, the degassing of xenon can safely be assumed to coincide with surface magmatism. Argon, another noble gas

\* Corresponding author.

E-mail address: [jun.korenaga@yale.edu](mailto:jun.korenaga@yale.edu) (J. Korenaga).

frequently used in the modeling of atmospheric evolution, may be chemically compatible with basaltic magma according to a recent experimental study (Watson et al., 2007), so modeling the degassing of argon requires greater care than previously given.

This paper is organized as follows. In the next section, we describe our theoretical formulation, in particular, how to combine the thermal evolution of the mantle with its chemical consequences in a self-consistent manner. Some model parameters suffer from nontrivial uncertainty, so after explaining typical model behavior with solution examples, we present results based on Monte Carlo sampling. Finally, we discuss previous studies on the coupled atmosphere–mantle evolution in light of our finding.

## 2. Model formulation

### 2.1. Thermal evolution of Earth

The thermal evolution of Earth is tracked backward in time from the present day, by integrating the following global energy balance (Christensen, 1985):

$$C \frac{dT_p(t)}{dt} = H(t) - Q(t), \quad (1)$$

where  $C$  is the heat capacity of the entire Earth ( $\sim 7 \times 10^{27} \text{ J K}^{-1}$ ),  $T_p$  is the mantle potential temperature (a hypothetical temperature of the mantle adiabatically brought up to the surface without melting),  $t$  is the time,  $H$  is the internal heat production in the mantle, and  $Q$  is the surface heat flux by mantle convection. The present-day potential temperature  $T_p(t_p)$  is assumed to be  $1350 \text{ }^\circ\text{C}$  (Herzberg et al., 2007). In this formulation, core heat flux is assumed to be proportional to the secular cooling of the mantle (Korenaga, 2008b, Section 3.5); the details of core evolution have only second-order effects on mantle evolution (Korenaga, 2008a).

Mantle heat production at the present day,  $H_m(t_p)$ , is the difference between the heat production of the bulk silicate Earth (BSE),  $16 \pm 3 \text{ TW}$  (Lyubetskaya and Korenaga, 2007b), and that of continental crust,  $7.5 \pm 2.5 \text{ TW}$  (Rudnick and Gao, 2003), i.e.,

$$H_m(t_p) = 16 - H_{cc}(t_p) + 3\varepsilon_1 \quad [\text{TW}], \quad (2)$$

where  $H_{cc}(t_p)$  is the present-day heat production in the continental crust,

$$H_{cc}(t_p) = 7.5 + 2.5\varepsilon_2 \quad [\text{TW}], \quad (3)$$

and  $\varepsilon_i$ 's are independent random variables with zero mean and unit standard deviation. Backtracking their values in the past is done by considering the radioactive decay of four heat-producing isotopes ( $^{238}\text{U}$ ,  $^{235}\text{U}$ ,  $^{232}\text{Th}$ , and  $^{40}\text{K}$ ) as in Korenaga (2006), except that we use  $\text{Th}/\text{U}=4$  and  $\text{K}/\text{U}=1.27 \times 10^4$  for both mantle and continental crust for simplicity. Mantle heat production through time may then be calculated by considering the effect of continental growth as

$$H(t) = H_m(t) + [1 - F_{cc}(t)]H_{cc}(t), \quad (4)$$

where  $F_{cc}$  is the mass fraction of continental crust with respect to the present-day value. Continental growth in the early Earth is still highly debated (e.g., Hawkesworth and Kemp, 2006; Harrison, 2009), so a range of possibilities spanning from the instantaneous growth model of Armstrong (1981),  $F_{cc}^A(t)$ , to the gradual growth model of McLennan and Taylor (1982),  $F_{cc}^{MT}(t)$ , is explored by randomizing a growth curve as

$$F_{cc}(t) = f_{\text{mix}} F_{cc}^A(t) + (1 - f_{\text{mix}}) F_{cc}^{MT}(t), \quad (5)$$

where  $f_{\text{mix}}$  is a random variable ranging from 0 to 1 (Fig. 1a).

The present-day mantle heat flux is the total terrestrial heat flux,  $46 \pm 3 \text{ TW}$  (Jaupart et al., 2007), minus the continental heat

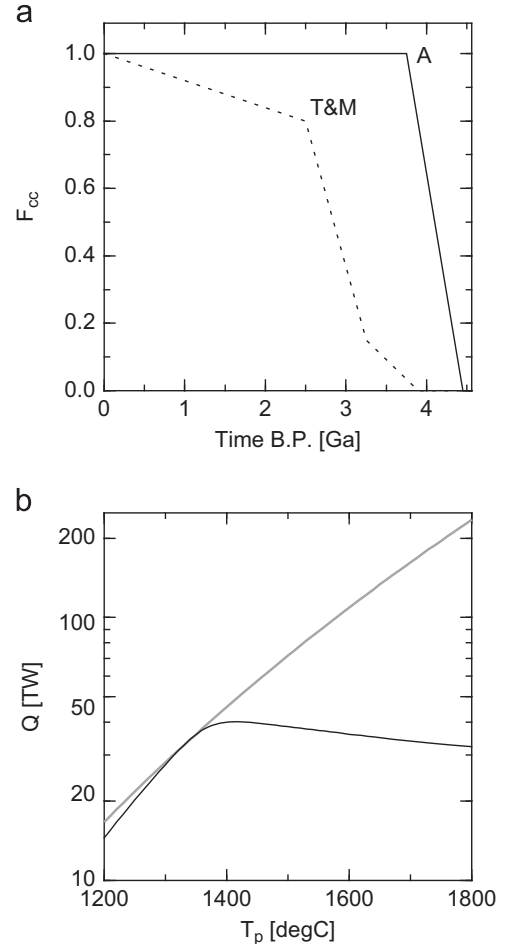


**Fig. 1.** (a) Two end-member models of continental growth used in this study: Armstrong (1981) (solid) and McLennan and Taylor (1982) (dotted). (b) Heat-flow scaling for mantle convection: Conventional (gray) and new (solid). Both are normalized here with the assumption of the present-day mantle heat flux of 36 TW at  $T_p$  of 13 500 °C. See Korenaga (2006) for the details of their derivations.

production, i.e.,

$$Q(t_p) = 46 - H_{cc}(t_p) + 3\varepsilon_3 \quad [\text{TW}], \quad (6)$$

where  $\varepsilon_3$  is another random variable with zero mean and unit standard deviation. The use of different random variables,  $\varepsilon_{1-3}$ , is to signify that the uncertainties of these observations are uncorrelated to each other. As in previous parameterized convection models, mantle heat flux in the past is modeled as a function of mantle potential temperature, and we consider both conventional and new scaling laws (Fig. 1b). In either case, a given scaling law is normalized so that it yields  $Q(t_p)$  as defined above for  $T_p(t_p)$  of  $1350 \text{ }^\circ\text{C}$ . For the new type of heat-flow scaling, a more refined approach has recently been developed (Korenaga, 2011), but for comparing the old and new scalings, this simplified approach is sufficient. The relative importance of mantle heat production over mantle heat flux may be quantified by the convective Urey ratio, which is defined as

$$Ur(t) = H(t)/Q(t). \quad (7)$$

Based on a relation between surface heat flux and plate velocity,  $Q \propto T_p \sqrt{V}$  (Turcotte and Schubert, 1982), average plate velocity may be calculated from mantle heat flux as

$$V(t) = V(t_p) \left( \frac{Q(t) T_p(t_p)}{Q(t_p) T_p(t)} \right)^2, \quad (8)$$

with the present-day velocity of  $5 \text{ cm yr}^{-1}$  (Parsons, 1981).

An example for thermal evolution with the new scaling is shown in Fig. 2 (solid curves), for which  $H_m(t_p) = 9.1$  TW,  $H_{cc}(t_p) = 5.4$  TW,  $Q(t_p) = 38.4$  TW, and  $f_{\text{mix}} = 0.56$  are used. The corresponding present-day Urey ratio is  $\sim 0.24$ , and the present-day BSE U concentration is 14.5 ppb. The reconstructed thermal history is concave downward, with a maximum at  $\sim 3.5$  Ga (Fig. 2a), because mantle heat production exceeds mantle heat flux prior to  $\sim 3.5$  Ga (Fig. 2b). This crossover between heat production and heat loss is made possible by more reduced heat

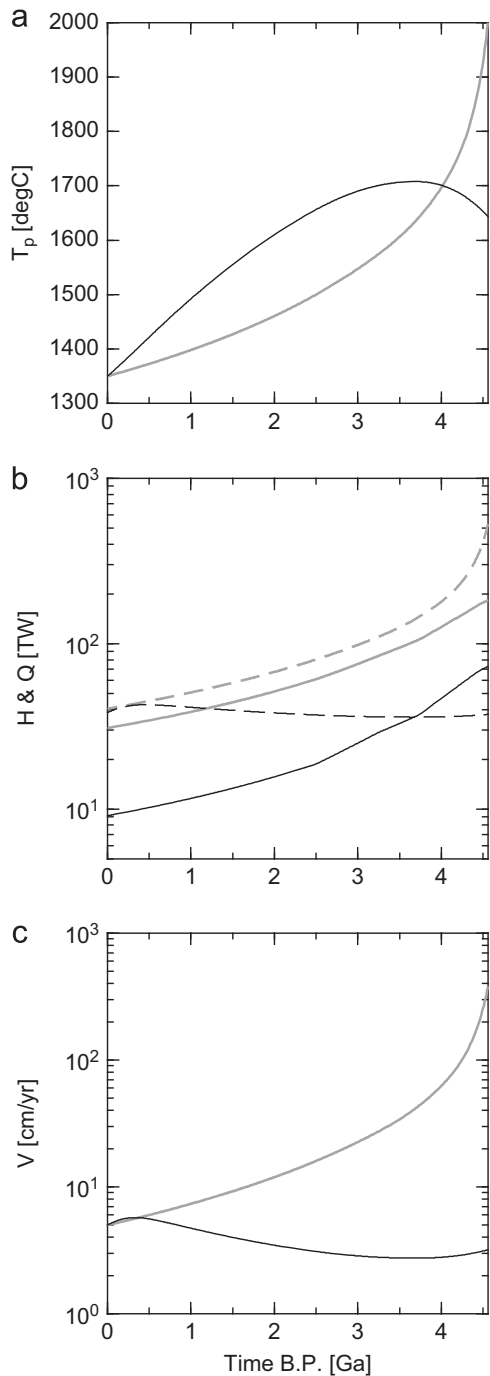


**Fig. 2.** Sample solutions from thermal evolution modeling: (a) mantle potential temperature  $T_p$ , (b) mantle heat production  $H$  (solid) and mantle heat flux  $Q$  (dashed), and (c) average plate velocity  $V$ , as a function of time before present. Gray and black curves are, respectively, for the cases with the conventional and new scalings.

flux for hotter mantle, and the effect of this new heat-flow scaling is also reflected in the evolution of average plate velocity (Fig. 2c).

With the new heat-flow scaling, it is always possible to reconstruct a geologically reasonable thermal history, similar to the one shown in Fig. 2, for any realization of the four random variables ( $\epsilon_{1-3}$  and  $f_{\text{mix}}$ ). With the conventional scaling, however, one cannot avoid an unrealistic, divergent history called ‘thermal catastrophe’ (Christensen, 1985) unless the mantle heat production  $H_m(t_p)$  is considerably higher than specified by geochemical constraints (Eq. (2)). When we use the conventional scaling, therefore, we first sample  $H_{cc}(t_p)$ ,  $Q(t_p)$ , and  $f_{\text{mix}}$  as in the case with the new scaling, and then seek by trial and error for an appropriate value of  $H_m(t_p)$ , which allows us to keep the potential temperature below 2500 °C throughout the Earth history. One example is shown in Fig. 2 (gray curves), for which  $H_m(t_p) = 30.9$  TW,  $H_{cc}(t_p) = 5.5$  TW,  $Q(t_p) = 40.4$  TW, and  $f_{\text{mix}} = 0.72$  are used. The present-day Urey ratio is  $\sim 0.77$  and the present-day BSE U concentration is 36.5 ppb in this case. The reconstructed thermal history is concave upward (Fig. 2a), and both mantle heat flux and plate velocity are considerably higher in the past than present (Fig. 2b,c). Thermal evolution with the conventional scaling is highly sensitive to the Urey ratio, and only a very narrow range of the present-day Urey ratio ( $\sim 0.75 \pm 0.05$ ) leads to geologically realistic solutions; slightly lower values give rise to thermal catastrophe, whereas slightly higher values result in a very cold initial mantle, e.g.,  $T_p(4.56 \text{ Ga}) < T_p(t_p)$  (cf. Figure 4 of Korenaga (2008b)).

In general, high Urey-ratio models predict a very hot start, whereas the low Urey-ratio models predict a relatively colder start, at the beginning of subsolidus mantle convection, i.e., the end of the crystallization of a putative magma ocean. These initial temperatures therefore do not directly reflect the temperature of the magma ocean during its main molten phase.

## 2.2. Xenon degassing

Thermal evolution described in the previous section affects how xenon could have degassed from the solid Earth in two different ways. First, the rate of degassing is controlled by the rate of mantle processing by magmatism, the temporal evolution of which depends on the histories of mantle potential temperature  $T_p(t)$  and plate velocity  $V(t)$ . Second, the spontaneous fission of  $^{238}\text{U}$  and  $^{244}\text{Pu}$  produces  $^{136}\text{Xe}$ , and the amount of xenon produced by this process is proportional to the amount of these parent isotopes. The thermal budget constrains the amount of  $^{238}\text{U}$  directly and that of  $^{244}\text{Pu}$  indirectly through the isotopic ratio  $^{244}\text{Pu}/^{238}\text{U}$ .

The degassing of xenon related to  $^{238}\text{U}$  may be modeled as follows. The amount of  $^{238}\text{U}$  in the mantle gradually decreases with time by radioactive decay as well as transport to the continental crust:

$$\frac{dN_{238\text{U}}^{\text{mantle}}(t)}{dt} = -\lambda_{238} N_{238\text{U}}^{\text{mantle}}(t) - \frac{C_{238\text{U}}^{\text{cc}}(t)}{m_{238}} \frac{dM_{\text{cc}}(t)}{dt}, \quad (9)$$

where  $N_{238\text{U}}^{\text{mantle}}$  is the number of  $^{238}\text{U}$  atoms in the mantle,  $\lambda_{238}$  and  $m_{238}$  are the decay constant and atomic mass of  $^{238}\text{U}$ , respectively,  $M_{\text{cc}}$  is the mass of continental crust,  $C_{238\text{U}}^{\text{cc}}$  is the concentration of  $^{238}\text{U}$  in the continental crust (as modeled when calculating  $H_{cc}(t)$  for thermal evolution). The evolution of uranogenic  $^{136}\text{Xe}$  in the mantle and in the atmosphere may then be modeled respectively as

$$\frac{dN_{136\text{Xe}}^{\text{mantle}}(t)}{dt} = \lambda_{238} Y_{238}^{136} N_{238\text{U}}^{\text{mantle}}(t) - N_{136\text{Xe}}^{\text{mantle}}(t) \frac{dF(t)}{dt}, \quad (10)$$

and

$$\frac{dN_{136\text{Xe}}^{\text{atm}}(t)}{dt} = N_{136\text{Xe}}^{\text{mantle}}(t) \frac{dF(t)}{dt}, \quad (11)$$

where  $Y_{238}^{136}$  is a probability of yielding  $^{136}\text{Xe}$  per one radioactive decay of  $^{238}\text{U}$ , and  $F$  is the mass fraction of the mantle processed by magmatism. Xenon is assumed to degas completely when the mantle is processed. The superscript \* on  $^{136}\text{Xe}$  denotes its radiogenic nature. In this geochemical box model with a single mantle reservoir, only one mantle composition can be handled, which is equivalent to assuming that any processed mantle is always homogenized with the rest of the mantle. Because we will focus on the present-day budget of atmospheric xenon, this simplified approach is acceptable as long as the entire mantle is predicted to have been processed at least once, which is indeed the case as shown later.

We consider two contributions to mantle processing. First, the mantle is processed by the formation of oceanic crust at mid-ocean ridges. The rate of mantle processing by this process may be given by

$$\frac{dM_{\text{proc}}^{\text{oc}}(t)}{dt} = \left( \frac{dM_{\text{proc}}^{\text{oc}}}{dt} \right)_{t_p} \frac{V(t)z_i(t)}{V(t_p)z_i(t_p)}, \quad (12)$$

where  $z_i$  denotes the initial depth of melting, which is controlled by mantle potential temperature as (Takahashi and Kushiro, 1983; Korenaga et al., 2002):

$$\rho_m g z_i(t) = \frac{T_p(t) - 1150}{120 \times 10^{-9} - (dT/dP)_S}. \quad (13)$$

Here  $\rho_m$  is mantle density ( $3300 \text{ kg m}^{-3}$ ),  $g$  is gravitational acceleration ( $9.8 \text{ m s}^{-2}$ ), and  $(dT/dP)_S$  is an adiabatic gradient in the shallow mantle. The present-day processing rate at mid-ocean ridges is estimated to be  $6.7 \times 10^{14} \text{ kg yr}^{-1}$  (Korenaga, 2006), which is based on  $V(t_p)$ ,  $z_i(t_p)$ , and the total length of divergent plate boundaries. The use of Eq. (12) does not readily imply that plate boundaries are assumed to be time-independent. Our velocity estimate with Eq. (8) assumes that the average aspect ratio of mantle convection cells is constant through time, and if plate sizes are smaller in the past, for example, predicted velocity has to become smaller than Eq. (8) indicates, in order to be consistent with heat-flow scaling. Thus, even a greater total ridge length (due to generally smaller plates) in the past does not lead to a notable deviation from what Eq. (12) predicts because plate velocity decreases at the same time. The model of mantle melting assumed in Eq. (13) is the same as that used for the new heat-flow scaling shown in Fig. 2b. Second, the mantle can also be processed for the formation of continental crust, and the rate of processing may be estimated as

$$\frac{dM_{\text{proc}}^{\text{cc}}(t)}{dt} = \frac{M_{\text{mantle}}}{N_{238\text{U}}^{\text{mantle}}(t)} \frac{C_{238\text{U}}^{\text{cc}}(t)}{m_{238}} \frac{dM_{\text{cc}}(t)}{dt}, \quad (14)$$

where  $M_{\text{mantle}}$  is the mass of the mantle. As indicated by Eq. (9), only the formation of continental crust affects the concentration of  $^{238}\text{U}$  in the mantle, because the oceanic crust is assumed to be recycled into the mantle by subduction, but for xenon degassing, both types of crustal genesis are relevant. The genesis of continental crust, however, may not be entirely independent from that of oceanic crust (e.g., Taylor and McLennan, 1995; Kelemen et al., 2003). If continental crust is produced by the secondary melting of oceanic crust, for example, the above consideration would lead to an overestimation of total mantle processing. We thus add these two contributions in the following way:

$$\frac{dF}{dt} = \frac{1}{M_{\text{mantle}}} \left( \frac{dM_{\text{proc}}^{\text{oc}}}{dt} + \max \left( \frac{dM_{\text{proc}}^{\text{cc}}}{dt} - \frac{dM_{\text{proc}}^{\text{oc}}}{dt}, 0 \right) \right). \quad (15)$$

That is, we consider mantle processing by continental growth only when mantle processing by mid-ocean ridge magmatism is insufficient to potentially explain the required mass transport to continental crust. The history of mantle processing corresponding to the examples in Fig. 2 is shown in Fig. 3. For the high Urey-ratio model with the conventional heat-flow scaling, the entire mantle is processed by mid-ocean ridge magmatism by  $\sim 10$  times over the Earth history, with half of its processing concentrated in the first  $\sim 500$  Myr (Fig. 3). In contrast, for the low Urey-ratio model with the new scaling, the mantle is processed about only once, and because mantle processing beneath mid-ocean ridges is more reduced, the second term of Eq. (15) becomes nonzero (Fig. 3, dashed).

The degassing of plutogenic  $^{136}\text{Xe}$  is modeled similarly, with the initial amount of  $^{244}\text{Pu}$  calculated from  $^{244}\text{Pu}/^{238}\text{U} = 0.0068$  at 4.56 Ga (Hudson et al., 1989). The half life of  $^{244}\text{Pu}$  is only 82 Myr, so its concentration in the mantle is controlled almost entirely by its radioactive decay. In addition to  $^{238}\text{U}$  and  $^{244}\text{Pu}$ , we also model the evolution of  $^{129}\text{I}$ , which decays to  $^{129}\text{Xe}$  with the half-life of 15.7 Myr, to increase the number of observational constraints. The number of differential equations to be solved is therefore 9 in total. Unlike thermal evolution modeling, we integrate these equations forward in time, starting at  $t_0 = 4.56$  Ga to present. Key model parameters are summarized in Table 1.

Our modeling of xenon degassing formulated above depends on thermal evolution modeling, which assumes the operation of subsolidus mantle convection through the Earth history. In the very early Earth, however, a completely different dynamical regime may exist because of a putative magma ocean (e.g., Solomatov, 2007). Such an early epoch is also considered to be characterized by an intense solar wind, which could have blown away most of Earth's primitive atmosphere (e.g., Pepin, 2006). Also, we have set  $t_0$  to 4.56 Ga, and this time corresponds to the beginning of the solar system (e.g., Halliday, 2003), not to the beginning of the fully grown Earth. Considerable loss of noble gases is expected during energetic planetary accretion processes. We thus introduce the closure time,  $t_c$ , to simulate these possibilities in the early solar system (e.g., Hamano and Ozima, 1978): Prior to  $t_c$ , we assume that all xenon produced in the mantle is entirely degassed and lost directly into space without being retained in the atmosphere.

Examples of xenon degassing corresponding to the two versions of thermal history (Fig. 2) are shown in Fig. 4. In both cases, the closure time  $t_c$  is chosen so that the prediction of the present-day amount of  $^{129}\text{Xe}^*$  in the atmosphere matches the observed value of  $1.7 \times 10^{35}$  atoms or  $2.8 \times 10^{11}$  mole (Porcelli and

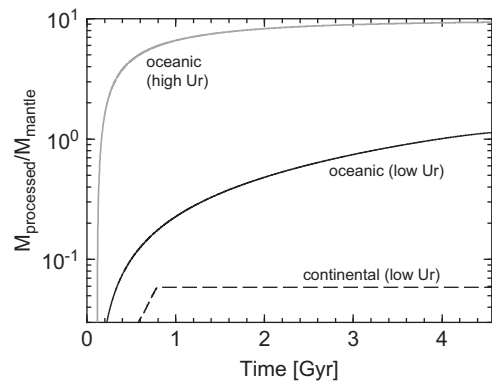


**Fig. 3.** Cumulative mass of processed mantle normalized by the mass of the whole mantle, corresponding to the sample solutions shown in Fig. 2. Here time is plotted starting from the beginning of the solar system (4.56 Ga) to the present. Mantle processing is very efficient for the high Urey-ratio model with the conventional scaling.

**Table 1**  
List of key model constants for xenon degassing.

Parameter	Definition	Value	Unit	Reference
$M_{\text{mantle}}$	Mass of the mantle	$4.0 \times 10^{24}$	kg	[1]
$M_{\text{cc}}$	Mass of the present-day continental crust	$2.4 \times 10^{22}$	kg	[1]
$\lambda_{238}$	Decay constant for $^{238}\text{U}$	0.155	$\text{Gyr}^{-1}$	[1]
$\lambda_{244}$	Decay constant for $^{244}\text{Pu}$	8.453	$\text{Gyr}^{-1}$	[1]
$\lambda_{129}$	Decay constant for $^{129}\text{I}$	44.15	$\text{Gyr}^{-1}$	[1]
$Y_{238}^{136}$	Fission yield of $^{136}\text{Xe}$ from $^{238}\text{U}$	$3.43 \times 10^{-8}$		[2]
$Y_{238}^{136}$	Fission yield of $^{136}\text{Xe}$ from $^{244}\text{Pu}$	$7.0 \times 10^{-5}$		[2]
$(^{244}\text{Pu}/^{238}\text{U})_{t_0}$	$^{244}\text{Pu}/^{238}\text{U}$ at 4.56 Ga	$0.0068 \pm 0.001$		[3]
$(^{129}\text{I}/^{127}\text{I})_{t_0}$	$^{129}\text{I}/^{127}\text{I}$ at 4.56 Ga	$1.1 \times 10^{-4}$		[4]
$C_{127\text{I}}^{\text{BSE}}$	Concentration of $^{127}\text{I}$ in bulk silicate Earth	13	ppb	[4]
$(dT/dP)_S$	Adiabatic gradient in the mantle	$1.54 \times 10^{-8}$	$\text{K Pa}^{-1}$	[5]
$(N_{^{129}\text{Xe}^*})_{\text{atm}}^{\text{atm}}$	Present-day atmospheric abundance of $^{129}\text{Xe}^*$	$1.7 \times 10^{35}$	atoms	[4]
$(N_{^{136}\text{Xe}^*})_{\text{atm}}^{\text{atm}}$	Present-day atmospheric abundance of $^{136}\text{Xe}^*$	$3.81 \times 10^{34}$	atoms	[4]

References: 1. Lodders and Fegley (1998), 2. Ozima and Podosek (2002), 3. Hudson et al. (1989), 4. Porcelli and Turekian (2003), and 5. Korenaga et al. (2002).

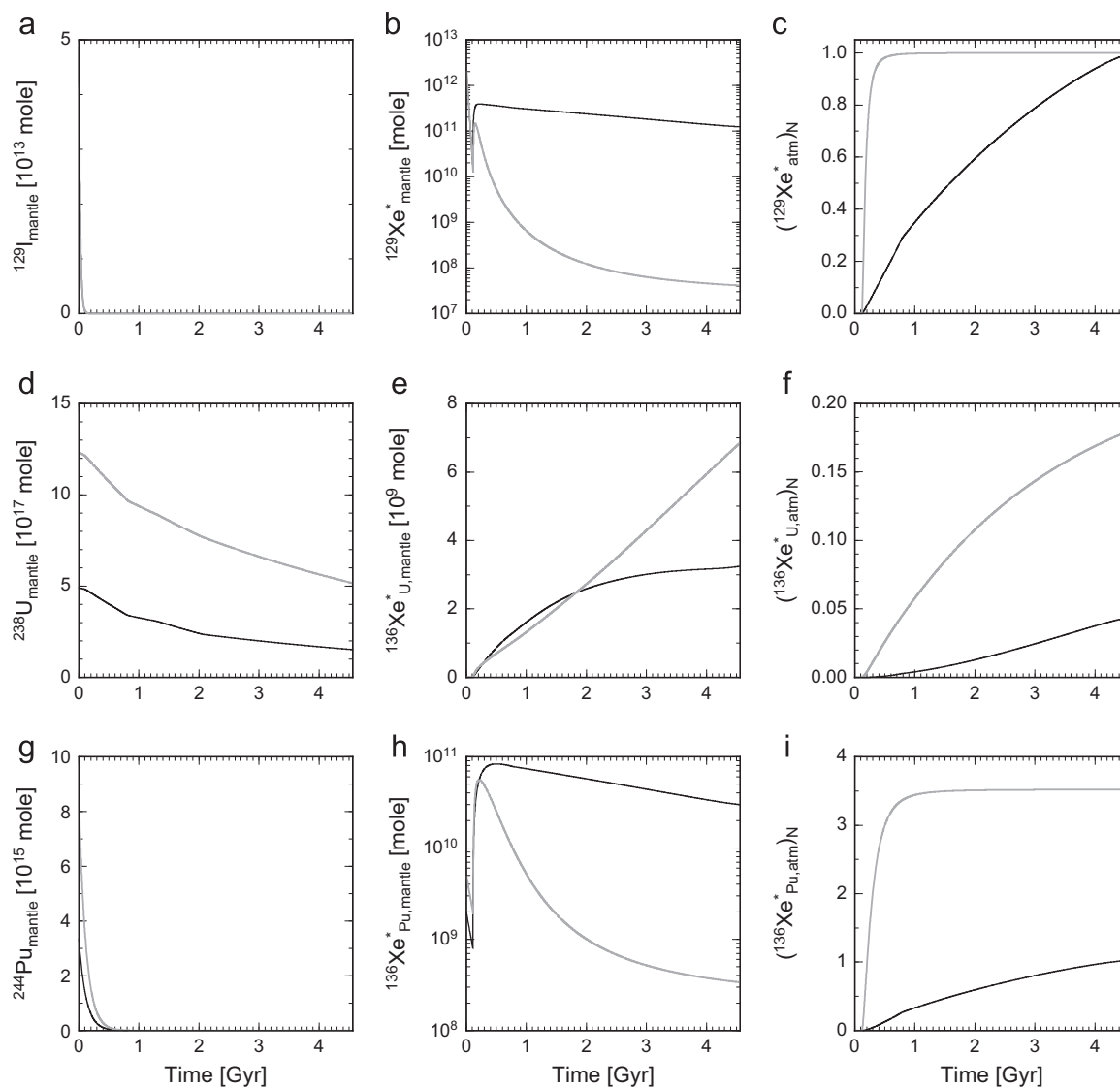


**Fig. 4.** Results for xenon degassing modeling corresponding to the thermal evolution models shown in Fig. 2. (a) The abundance of  $^{129}\text{I}$  in the mantle, (b) the abundance of  $^{129}\text{Xe}$  in the mantle, (c) the relative abundance of  $^{129}\text{Xe}^*$  in the atmosphere normalized by the observed present-day value, (d) the abundance of  $^{238}\text{U}$  in the mantle, (e) the abundance of uraniumogenic  $^{136}\text{Xe}^*$  in the mantle, (f) the relative abundance of uraniumogenic  $^{136}\text{Xe}^*$  in the atmosphere normalized by the observed value of  $^{136}\text{Xe}^*$ , (g) the abundance of  $^{244}\text{Pu}$  in the mantle, (h) the abundance of plutogenic  $^{136}\text{Xe}^*$  in the mantle, and (i) the relative abundance of plutogenic  $^{136}\text{Xe}^*$  in the atmosphere normalized by the observed value of  $^{136}\text{Xe}^*$ . As in Figs. 2 and 3, gray and black curves denote high and low Urey-ratio models, respectively.

Turekian, 2003) (Fig. 4c). In these examples, the closure times are 108 Myr and 115 Myr, respectively, for the low and high Urey-ratio models. Because of its short half-life,  $^{129}\text{I}$  in the mantle is essentially depleted within the closure time, unaffected by subsequent mantle dynamics (Fig. 4a). The initial amount of  $^{129}\text{I}$  is unrelated to the abundance of  $^{238}\text{U}$  or other heat-producing isotopes and therefore the same for both low and high Urey-ratio models, but the fate of its decay product  $^{129}\text{Xe}^*$  in the mantle is quite different between these models (Fig. 4b). The closure time has to be slightly greater for the high Urey-ratio model because of its very efficient mantle processing in the early Earth (Fig. 3); otherwise the present-day atmospheric abundance of  $^{129}\text{Xe}^*$  would be overpredicted.

Compared to the low Urey-ratio model with the new heat-flow scaling, the high Urey-ratio model has greater amounts of initial  $^{238}\text{U}$  and  $^{244}\text{Pu}$  (Fig. 4d,g) and also processes the mantle more efficiently (Fig. 4h,h), resulting in the a considerable amount of  $^{136}\text{Xe}^*$  in the present-day atmosphere ( $> 3$  times more than required by observation; see Fig. 4f,i). If one increases  $t_c$  to remove this discrepancy, the predicted amount of  $^{129}\text{Xe}^*$  would then become too small. The two versions of thermal evolution, therefore, lead to very different predictions for xenon degassing.

### 3. Results

Our overall strategy for the coupled thermal and chemical evolution modeling is the following (Fig. 5). For each type of heat-flow scaling, we explore the uncertainty of the present-day thermal budget and that of continental growth by randomly sampling four parameters  $\varepsilon_{1-3}$  and  $f_{\text{mix}}$  from their a priori ranges

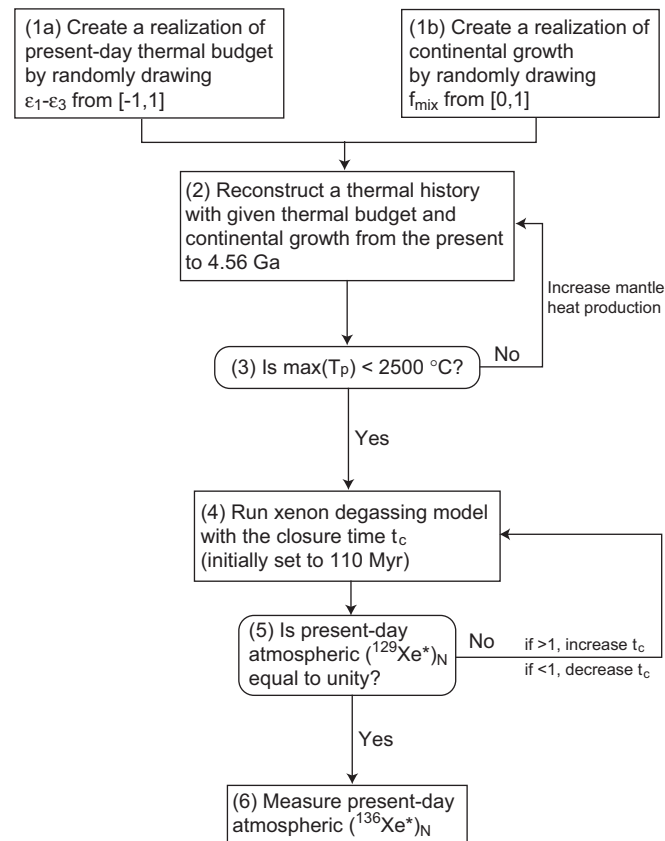


Fig. 5. Flow chart of coupled atmosphere–mantle evolution modeling implemented in this study.

( $[-1, 1]$  and  $[0, 1]$ , respectively), though, as already discussed in the previous section, the parameter  $\varepsilon_1$  for mantle heat production has to be considerably greater than unity in case of the conventional scaling. For each random realization of a thermal history, we then seek a corresponding degassing history by adjusting the closure time  $t_c$ , so that the predicted atmospheric abundance of  $^{129}\text{Xe}^*$  at present matches the observed value. With a binary search algorithm, such a closure time can be found by several iterations. With this approach, the present-day amount of  $^{136}\text{Xe}^*$  in the atmosphere cannot be matched exactly, so a relative deviation from the observed value is measured to quantify the success of each model run. A key variable in the degassing part is  $(^{244}\text{Pu}/^{238}\text{U})_{t_0}$ , which relates the thermal budget with the atmospheric xenon budget. This isotopic ratio is estimated to be  $0.0068 \pm 0.001$  (i.e.,  $\sim 15\%$  uncertainty), but this is based on a single meteorite (Hudson et al., 1989), so the reported uncertainty is better regarded as a minimum estimate (cf. Turner et al., 2007). We explore the effect of this uncertainty by using three values of  $(^{244}\text{Pu}/^{238}\text{U})_{t_0}$ , 0.0058, 0.0068, and 0.0078. Another source of uncertainty is related to the iodine budget (e.g., Porcelli and Turekian, 2003), but because the half-life of  $^{129}\text{I}$  is considerably shorter than that of  $^{244}\text{Pu}$ , the uncertainty of the iodine budget merely results in minor variations in the closure time and has little impact on the predicted  $^{136}\text{Xe}^*$  budget.

For both types of heat-flow scaling, we generate  $10^3$  Monte Carlo realizations of thermal history, and for each realization of thermal history, we obtained a corresponding degassing history with three values of  $(^{244}\text{Pu}/^{238}\text{U})_{t_0}$ . The total number of simulated degassing histories is therefore  $6 \times 10^3$ , and the results of these simulations are summarized in Fig. 6. The conventional heat-flow scaling requires the present-day Urey ratio to be in the range of 0.7 to 0.8, and the concave-upward nature of predicted thermal history (Fig. 2a) results in a wide spread of the maximum mantle temperature, which corresponds to the beginning of the Earth history, whereas the mantle temperature at 3 Ga is tightly clustered around  $1550^\circ\text{C}$  (Fig. 6a). With the new heat-flow scaling, a geologically reasonable thermal history can be constructed with much lower Urey ratios ( $\sim 0.1$  to  $\sim 0.35$ ), which are consistent with the geochemical models of Earth composition (e.g., McDonough and Sun, 1995; Lyubetskaya and Korenaga, 2007a). Because of concave-downward thermal evolution (Fig. 2a), there is only small difference between the mantle temperature at 3 Ga and the maximum temperature (Fig. 6a).

The closure time for the high Urey-ratio models is uniformly 115 Myr, whereas that for the low Urey-ratio models is distributed in a range of 106 to 112 Myr (Fig. 6b). Because the low Urey-ratio models process the mantle more gradually (Fig. 3), the present-day atmospheric  $^{129}\text{Xe}^*$  budget is sensitive to the entire Earth history (Fig. 4c), including the details of continental growth. This sensitivity results in the scatter in the closure time. As mentioned in the previous section, the closure time has to be greater for the high Urey-ratio models because mantle processing is much more efficient with the conventional scaling. Considering the 15% uncertainty of the solar system initial,  $(^{244}\text{Pu}/^{238}\text{U})$  at the time of closure (106–115 Myr) is  $0.0027 \pm 0.0005$ , which encompasses the previous estimate of 0.0026 (Ozima and Podosek, 2002, p. 238).

With  $(^{244}\text{Pu}/^{238}\text{U})_{t_0}$  of 0.0058, the low Urey-ratio models can correctly predict the present-day atmospheric budget of  $^{136}\text{Xe}^*$ , and even with  $(^{244}\text{Pu}/^{238}\text{U})_{t_0}$  of 0.0078, it overpredicts only by  $\sim 50\%$  (Fig. 6c). In contrast, the high Urey-ratio models overpredict the  $^{136}\text{Xe}^*$  budget by more than  $\sim 300\%$ . The ultimate cause of this gross overprediction is the use of conventional scaling. This scaling itself predicts very efficient mantle processing when the mantle was hotter in the past, and it also requires high Urey ratios, which lead to high initial abundances of  $^{244}\text{Pu}$ .

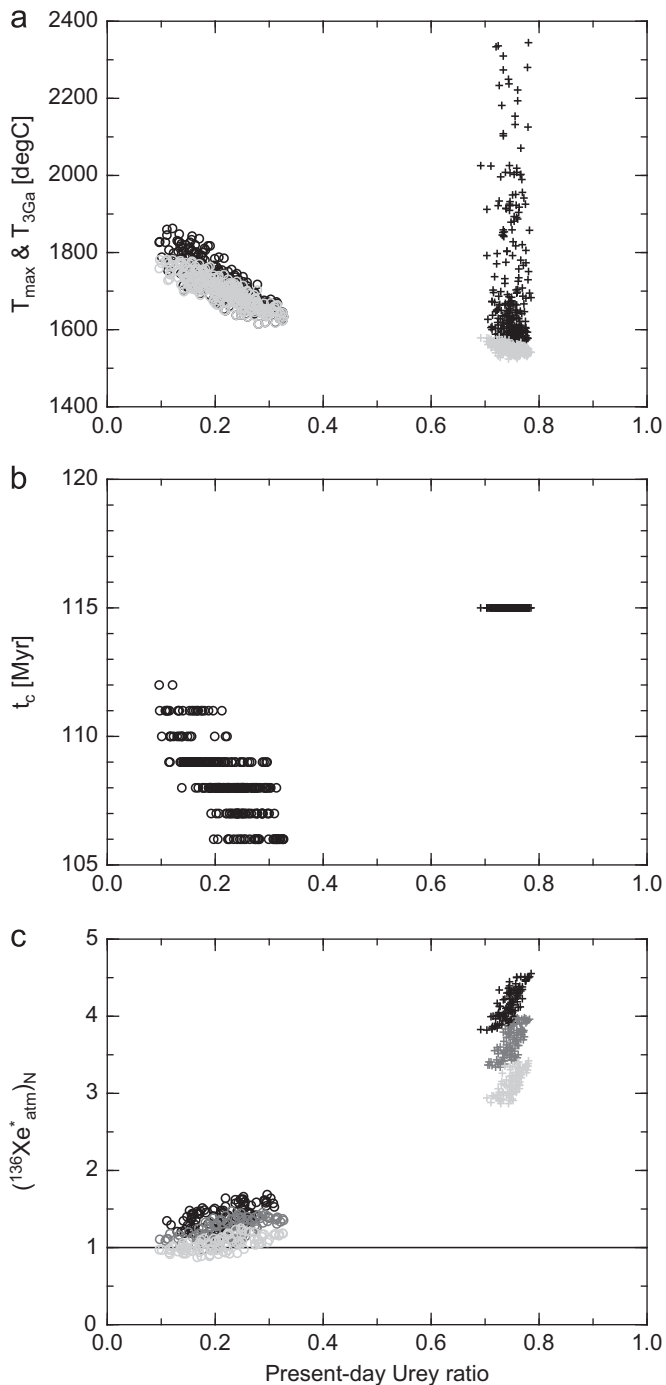


**Fig. 6.** Summary of modeling results for coupled atmosphere–mantle evolution based on  $6 \times 10^3$  Monte Carlo realizations. (a) Maximum mantle temperature (solid symbols) and mantle temperature at 3 Ga (gray symbols), (b) closure time  $t_c$ , and (c) the relative abundance of  $^{136}\text{Xe}^*$  in the present-day atmosphere normalized by the observed value (light gray, gray, and solid symbols are, respectively, for the cases with  $(^{244}\text{Pu}/^{238}\text{U})_{t_0}$  of 0.0058, 0.0068, and 0.0078), shown as a function of the present-day Urey ratio. Circles and crosses are for the cases with new and conventional scalings, respectively.

#### 4. Discussion and conclusion

Our formulation for thermal evolution and mantle degassing is admittedly simplistic, but this intentional simplicity highlights how different assumptions on heat-flow scaling lead to different geochemical consequences. The complete degassing of xenon directly to space before the closure time  $t_c$ , for example, may not happen in reality, but we believe that the effects of magma

ocean and intense solar wind in the very early Earth can be captured approximately by this sort of effective closure time. Also, the use of a particular heat-flow scaling for the entire subsequent history implies the operation of plate tectonics since the Hadean, and this is a highly controversial topic (e.g., [Condie and Pease, 2008](#); [Hopkins et al., 2010](#)). Regardless of the details of what actually happened, however, comparing both types of heat-flow scaling allowed us to explore two contrasting early Earth conditions, and we hope that a more realistic situation may be bounded by these end-members.

What is important in our approach is (1) a self-consistent combination of thermal evolution and xenon degassing and (2) a proper pairing of model parameterization and observational constraints. These issues may be best explained by comparing our study with a recent study by [Coltice et al. \(2009\)](#), who also studied the degassing of xenon by combining geochemical box modeling with thermal evolution. First, [Coltice et al. \(2009\)](#) explored a range of thermal histories from concave-upward to concave-downward (see their Fig. 2), but they varied a thermal history independently from the geochemical budget. As one may understand from Fig. 2a, however, the curvature of a thermal history is closely related to the thermal budget and heat-flow scaling. To have a concave-upward thermal history (or to keep a relatively low rate of secular cooling during the last  $\sim 2$  Gyr, for example, the present-day Urey ratio has to be sufficiently high, which is equivalent to a high abundance of  $^{238}\text{U}$  and thus  $^{244}\text{Pu}$ . This is a robust consequence of the global energy balance (Eq. (1)). When exploring a range of thermal histories, therefore, the geochemical budget has to be varied in a self-consistent manner. Second, [Coltice et al. \(2009\)](#) judged the success of modeling results based solely on predicted present-day values for  $^{136}\text{Xe}_{\text{Pu}}^*/^{136}\text{Xe}_{\text{U}}^*$  and  $^{129}\text{Xe}^*/^{136}\text{Xe}_{\text{Pu}}^*$  in the mantle, which have been estimated to be 0.4–1.5 and 1–10, respectively, by [Yokochi and Marty \(2005\)](#). These estimates are, however, model-dependent and based primarily on samples from one geographic location (the Kola peninsula), so it is unclear how closely these numbers may resemble the true mantle-average isotopic ratios. Previous studies on xenon isotopes suggest that xenon presently found in the upper mantle may not be a simple residue from the degassing of the atmosphere (e.g., [Ozima and Podosek, 2002](#); [Porcelli and Turekian, 2003](#)), and the convecting mantle is expected to be isotopically heterogeneous at a variety of scales (e.g., [Zindler and Hart, 1986](#)). The geochemical box modeling of [Coltice et al. \(2009\)](#) treats the whole mantle as one uniform reservoir (as is done in this study), so in order to test its prediction for mantle values, appropriate observational constraints have to mantle-average values, which are difficult to obtain for xenon isotopes. This is why we focus on the prediction for atmospheric xenon in this study. As explained in Section 2.2, treating the whole mantle as a homogenized reservoir is acceptable as long as the entire mantle is predicted to have been processed by magmatism at least once, because we consider only the present-day amount of the degassed component. The bulk majority of atmospheric  $^{136}\text{Xe}^*$  originates in  $^{244}\text{Pu}$ , the short half-life of which means that the production of  $^{136}\text{Xe}_{\text{Pu}}^*$  in the mantle was complete in the first few hundred million years (Fig. 4). Because  $^{238}\text{U}$  has a much longer half-life, however, the evolution of  $^{136}\text{Xe}_{\text{U}}^*/^{136}\text{Xe}_{\text{Pu}}^*$  at a given location in the mantle depends on the detail of how the mantle has been processed and mixed in the past. In contrast, the total amount of  $^{136}\text{Xe}_{\text{Pu}}^*$  degassed into the atmosphere depends simply on the efficiency of mantle processing. Evaluating the success of a given model, therefore, has to take into account how the model is parameterized, to avoid comparing apples and oranges.

We divided the Earth history into two phases by the closure time, and complete degassing is assumed during the earlier phase.

In fact, intense degassing from the very early Earth, followed by more subdued degassing history, has been repeatedly suggested by the studies of noble gases (e.g., Hamano and Ozima, 1978; Allegre et al., 1987), so this is nothing new. What is new is the realization that the subsequent more gradual degassing is incompatible with the conventional thermal evolution models, which have a long tradition in geophysics. One may try to rescue the conventional scaling by postulating layered-mantle convection to suppress xenon degassing, but the kind of layered-mantle convection that can yield a geologically reasonable thermal history is characterized by an enriched upper mantle and a depleted lower mantle (Spohn and Schubert, 1982; Honda, 1995), which is entirely opposite to what is commonly favored in geochemistry (e.g., Allegre et al., 1996; Albarede and van der Hilst, 2002) and does not reduce xenon degassing at all. Layered-mantle models thus have to be more convoluted than usually thought, in order to satisfy both geophysical and geochemical constraints. The notion of more sluggish plate tectonics, as suggested by the new heat-flow scaling, predicts inefficient mantle processing, and in terms of bulk Earth predictions, it may be equivalent to conventional layered-mantle models with an enriched, more sluggish lower mantle. It would be interesting to elaborate the geochemical part to have more than one mantle reservoir so that we can evaluate the effect of mantle mixing (e.g., Kellogg et al., 2007; Gonnermann and Mukhopadhyay, 2009). Also, our approach of coupling thermal and chemical evolutions can be in principle extended to include other noble gases, and such simultaneous modeling of noble gases (e.g., Porcelli and Wasserburg, 1995b, 1995a) would be essential to address the evolution of Earth's atmosphere in a more comprehensive manner. When doing so, it will become important to consider factors other than degassing, such as contributions from late veneers, in order to resolve the missing xenon problem (Ozima and Podosek, 1999; Dauphas, 2003; Pepin, 2006).

In this regard, it would be interesting to point out a close connection between this study and the studies of Sleep (1979) and Tajika and Matsui (1993), who investigated how the degassing of  $^{40}\text{Ar}$  may constrain the thermal evolution of Earth. Both of these studies concluded that in order to satisfy both the mantle budget of  $^{40}\text{K}$  (the parent isotope of  $^{40}\text{Ar}$ ) and the atmospheric budget of  $^{40}\text{Ar}$ , the past intensity of mantle convection and thus its processing should have been similar to the present-day level, which is essentially identical to our conclusion in this study. A more popular interpretation of the atmospheric argon is, however, that mantle processing has been insufficient because of the layered mantle (e.g., Allegre et al., 1996), though such layered mantle does not produce a physically viable thermal evolution as already mentioned. The interpretation of the atmospheric argon has recently been complicated by the experimental work of Watson et al. (2007), who suggest that argon does not degas by mid-ocean-ridge magmatism, though this experimental study needs further verification (e.g., Cassata et al., 2011). If argon were incompatible with basaltic melt as traditionally thought, the overall consistency of our study with Sleep (1979) and Tajika and Matsui (1993) would strengthen our conclusion on the evolution of mantle convection.

The possibility of more sluggish plate tectonics in the past was originally raised to reconcile the physical evolution of Earth with geochemical constraints on the present-day thermal budget (Korenaga, 2003). It has since been shown that the geological record of ancient passive margins is consistent with reduced plate velocity in the past (Bradley, 2008) and that the petrological reconstruction of mantle potential temperature up to  $\sim 3.5$  Ga indicates a concave-downward thermal history (Herzberg et al., 2010). We suggest that the present-day atmospheric budget of radiogenic xenon also favors this new view on the evolution of plate tectonics through the Earth history.

## Acknowledgments

This work was sponsored by Microsoft A. Richard Newton Breakthrough Research Award. The authors thank the Editor Mark Harrison and two anonymous reviewers for constructive comments.

## References

- Albarède, F., 1998. Time-dependent models of U-Th-He and K-Ar evolution and the layering of mantle convection. *Chem. Geol.* 145, 413–429.
- Albarede, F., van der Hilst, R.D., 2002. Zoned mantle convection. *Phil. Trans. R. Soc. Lond. A* 360, 2569–2592.
- Allegre, C.J., Hofmann, A., O'Nions, K., 1996. The argon constraints on mantle structure. *Geophys. Res. Lett.* 23, 3555–3557.
- Allegre, C.J., Staudacher, T., Sarda, P., 1987. Rare gas systematics: formation of the atmosphere, evolution and structure of the Earth's mantle. *Earth Planet. Sci. Lett.* 81, 127–150.
- Armstrong, R.L., 1981. Radiogenic isotopes: the case for crustal recycling on a near-steady-state no-continental-growth Earth. *Phil. Trans. R. Soc. Lond. A* 301, 443–472.
- Bradley, D.C., 2008. Passive margins through earth history. *Earth-Sci. Rev.* 91, 1–26.
- Cassata, W.S., Renne, P.R., Shuster, D.L., 2011. Argon diffusion in pyroxenes: implications for thermochronometry and mantle degassing. *Earth Planet. Sci. Lett.* 304, 407–416.
- Christensen, U.R., 1985. Thermal evolution models for the Earth. *J. Geophys. Res.* 90, 2995–3007.
- Coltice, N., Marty, B., Yokochi, R., 2009. Xenon isotope constraints on the thermal evolution of the early Earth. *Chem. Geol.* 266, 4–9.
- Condie, K.C., Pease, V. (Eds.), 2008. *When Did Plate Tectonics Begin on Planet Earth?* Geological Society of America.
- Dauphas, N., 2003. The dual origin of the terrestrial atmosphere. *Icarus* 165, 326–339.
- Davies, G.F., 1980. Thermal histories of convective Earth models and constraints on radiogenic heat production in the earth. *J. Geophys. Res.* 85, 2517–2530.
- Gonnermann, H.M., Mukhopadhyay, S., 2009. Preserving noble gases in a convecting mantle. *Nature* 459, 560–563.
- Halliday, A.N., 2003. The origin and earliest history of the earth. In: Holland, H.D., Turekian, K.K. (Eds.), *Treatise on Geochemistry*, vol. 1. Elsevier, pp. 509–557.
- Hamano, Y., Ozima, M., 1978. Earth-atmosphere evolution model based on Ar isotopic data. In: E.C. Alexander, J., Ozima, M. (Eds.), *Terrestrial Rare Gases*. Japan Scientific Societies Press, pp. 155–171.
- Harrison, T.M., 2009. The Hadean crust: evidence from  $> 4$  Ga zircon. *Annu. Rev. Earth Planet. Sci.* 37, 479–505.
- Hawkesworth, C.J., Kemp, A.I.S., 2006. Evolution of the continental crust. *Nature* 443, 811–817.
- Herzberg, C., Asimow, P.D., Arndt, N., Niu, Y., Leshner, C.M., Fitton, J.G., Cheadle, M.J., Saunders, A.D., 2007. Temperatures in ambient mantle and plumes: constraints from basalts, picrites, and komatiites. *Geochem. Geophys. Geosys.* 8 (2), Q02206, <http://dx.doi.org/10.1029/2006GC001390>.
- Herzberg, C., Condie, K., Korenaga, J., 2010. Thermal evolution of the Earth and its petrological expression. *Earth Planet. Sci. Lett.* 292, 79–88.
- Honda, S., 1995. A simple parameterized model of Earth's thermal history with the transition from layered to whole-mantle convection. *Earth Planet. Sci. Lett.* 131, 357–369.
- Hopkins, M.D., Harrison, T.M., Manning, C.E., 2010. Constraints on Hadean geodynamics from mineral inclusions in  $> 4$  Ga zircons. *Earth Planet. Sci. Lett.* 298, 367–376.
- Hudson, G.B., Kennedy, B.M., Podosek, F.A., Hohenberg, C.M., 1989. The early solar system abundance of  $^{244}\text{Pu}$  as inferred from the St. Severin chondrite. In: *Proceedings of the 19th Lunar and Planetary Science Conference*, 1989, pp. 547–557.
- Jaupart, C., Labrosse, S., Mareschal, J.-C., 2007. Temperatures, heat and energy in the mantle of the Earth. In: Schubert, G. (Ed.), *Treatise on Geophysics*, vol. 7. Elsevier, Amsterdam, pp. 253–303.
- Kelemen, P.B., Hanghøj, K., Greene, A.R., 2003. One view of the geochemistry of subduction-related magmatic arcs, with an emphasis on primitive andesite and lower crust. In: Holland, H.D., Turekian, K.K. (Eds.), *Treatise on Geochemistry*, vol. 3. Elsevier, Amsterdam, pp. 593–659.
- Kellogg, J.B., Jacobsen, S.B., O'Connell, R.J., 2007. Modeling lead isotopic heterogeneity in mid-ocean ridge basalts. *Earth Planet. Sci. Lett.* 262, 328–342.
- Korenaga, J., 2003. Energetics of mantle convection and the fate of fossil heat. *Geophys. Res. Lett.* 30, 1437, <http://dx.doi.org/10.1029/2003GL016982>.
- Korenaga, J., 2006. Archean geodynamics and the thermal evolution of Earth. In: Benn, K., Mareschal, J.-C., Condie, K. (Eds.), *Archean Geodynamics and Environments*. American Geophysical Union, Washington, D.C., pp. 7–32.
- Korenaga, J., 2008a. Plate tectonics, flood basalts, and the evolution of Earth's oceans. *Terra Nova* 20, 419–439.
- Korenaga, J., 2008b. Urey ratio and the structure and evolution of Earth's mantle. *Rev. Geophys.* 46, RG2007, <http://dx.doi.org/10.1029/2007RG000241>.
- Korenaga, J., 2011. Thermal evolution with a hydrating mantle and the initiation of plate tectonics in the early Earth. *J. Geophys. Res.* 116, B12403, <http://dx.doi.org/10.1029/2011JB008410>.

- Korenaga, J., Kelemen, P.B., Holbrook, W.S., 2002. Methods for resolving the origin of large igneous provinces from crustal seismology. *J. Geophys. Res.* 107 (B9), 2178, <http://dx.doi.org/10.1029/2001JB001030>.
- Lodders, K., Fegley, B., 1998. *The Planetary Scientist's Companion*. Oxford University Press, New York.
- Lyubetskaya, T., Korenaga, J., 2007a. Chemical composition of Earth's primitive mantle and its variance, 1, methods and results. *J. Geophys. Res.* 112, B03211, <http://dx.doi.org/10.1029/2005JB004223>.
- Lyubetskaya, T., Korenaga, J., 2007b. Chemical composition of Earth's primitive mantle and its variance, 2, implications for global geodynamics. *J. Geophys. Res.* 112, B03212, <http://dx.doi.org/10.1029/2005JB004224>.
- McDonough, W.F., Sun, S.-S., 1995. The composition of the Earth. *Chem. Geol.* 120, 223–253.
- McLennan, S.M., Taylor, R.S., 1982. Geochemical constraints on the growth of the continental crust. *J. Geol.* 90, 347–361.
- Ozima, M., Podosek, F.A., 1999. Formation age of Earth from  $^{129}\text{I}/^{127}\text{I}$  and  $^{244}\text{Pu}/^{238}\text{U}$  systematics and the missing Xe. *J. Geophys. Res.* 104, 25493–25499.
- Ozima, M., Podosek, F.A., 2002. *Noble Gas Geochemistry*. 2nd edn., Cambridge.
- Parsons, B., 1981. The rates of plate creation and consumption. *Geophys. J. R. Astron. Soc.* 67, 437–448.
- Pepin, R.O., 2006. Atmospheres on the terrestrial planets: clues to origin and evolution. *Earth Planet. Sci. Lett.* 252, 1–14.
- Porcelli, D., Turekian, K.K., 2003. The history of planetary degassing as recorded by noble gases. In: Holland, H.D., Turekian, K.K. (Eds.), *Treatise on Geochemistry*, vol. 4. Elsevier, pp. 281–318.
- Porcelli, D., Wasserburg, G.J., 1995a. Mass transfer of helium, neon, argon, and xenon through a steady-state upper mantle. *Geochim. Cosmochim. Acta* 59, 4921–4937.
- Porcelli, D., Wasserburg, G.J., 1995b. Mass transfer of xenon through a steady-state upper mantle. *Geochim. Cosmochim. Acta* 59, 1991–2007.
- Rudnick, R.L., Gao, S., 2003. Composition of the continental crust. In: Holland, H.D., Turekian, K.K. (Eds.), *Treatise on Geochemistry*, vol. 3. Elsevier, pp. 1–64.
- Schubert, G., Stevenson, D., Cassen, P., 1980. Whole planet cooling and the radiogenic heat source contents of the earth and moon. *J. Geophys. Res.* 85, 2531–2538.
- Schubert, G., Turcotte, D.L., Olson, P., 2001. *Mantle Convection in the Earth and Planets*. Cambridge, New York.
- Sleep, N.H., 1979. Thermal history and degassing of the Earth: some simple calculations. *J. Geol.* 87, 671–686.
- Solomatov, V., 2007. Magma oceans and primordial mantle differentiation. In: Schubert, G. (Ed.), *Treatise on Geophysics*, vol. 9. Elsevier, pp. 91–119.
- Spohn, T., Schubert, G., 1982. Modes of mantle convection and the removal of heat from the Earth's interior. *J. Geophys. Res.* 87, 4682–4696.
- Tajika, E., Matsui, T., 1993. Evolution of seafloor spreading rate based on  $^{40}\text{Ar}$  degassing history. *Geophys. Res. Lett.* 20, 851–854.
- Takahashi, E., Kushiro, I., 1983. Melting of a dry peridotite at high pressures and basalt magma genesis. *Am. Mineral.* 68, 859–879.
- Taylor, S.R., McLennan, S.M., 1995. The geochemical evolution of the continental crust. *Rev. Geophys.* 33, 241–265.
- Turcotte, D.L., Schubert, G., 1982. *Geodynamics: Applications of Continuum Physics to Geological Problems*. John Wiley, New York.
- Turner, G., Busfield, A., Crowther, S.A., Harrison, M., Mojzsis, S.J., Gilmour, J., 2007. Pu-Xe, U-Xe, U-Pb chronology and isotope systematics of ancient zircons from Western Australia. *Earth Planet. Sci. Lett.* 261, 491–499.
- Watson, E.B., Thomas, J.B., Cherniak, D.J., 2007.  $^{40}\text{Ar}$  retention in the terrestrial planets. *Nature* 449, 299–304.
- Williams, D.R., Pan, V., 1992. Internally heated mantle convection and the thermal and degassing history of the Earth. *J. Geophys. Res.* 97, 8937–8950.
- Yokochi, R., Marty, B., 2005. Geochemical constraints on mantle dynamics in the Hadean. *Earth Planet. Sci. Lett.* 238, 17–30.
- Zindler, A., Hart, S., 1986. Chemical geodynamics. *Annu. Rev. Earth Planet. Sci.* 14, 493–571.